Subsite Mapping of the Human Pancreatic α-Amylase Active Site through Structural, Kinetic, and Mutagenesis Techniques[†,‡]

Gary D. Brayer,[*,§] Gary Sidhu,[§] Robert Maurus,[§] Edwin H. Rydberg,[§] Curtis Braun,[||] Yili Wang,[§] Nham T. Nguyen,[§] Christopher M. Overall,[§,⊥] and Stephen G. Withers[§,||]

Department of Biochemistry and Molecular Biology, University of British Columbia, Vancouver V6T 1Z3, Canada, Department of Chemistry, University of British Columbia, Vancouver V6T 1Z1, Canada, and Department of Oral Biological and Medical Sciences, University of British Columbia, Vancouver V6T 1Z3, Canada

Received September 9, 1999; Revised Manuscript Received November 30, 1999

ABSTRACT: We report a multifaceted study of the active site region of human pancreatic α-amylase. Through a series of novel kinetic analyses using malto-oligosaccharides and malto-oligosaccharyl fluorides, an overall cleavage action pattern for this enzyme has been developed. The preferred binding/cleavage mode occurs when a maltose residue serves as the leaving group (aglycone sites +1 and +2) and there are three sugars in the glycon (−1, −2, −3) sites. Overall it appears that five binding subsites span the active site, although an additional glycon subsite appears to be a significant factor in the binding of longer substrates. Kinetic parameters for the cleavage of substrates modified at the 2 and 4″ positions also highlight the importance of these hydroxyl groups for catalysis and identify the rate-determining step. Further kinetic and structural studies pinpoint Asp197 as being the likely nucleophile in catalysis, with substitution of this residue leading to an $\sim 10^6$-fold drop in catalytic activity. Structural studies show that the original pseudo-tetrasaccharide structure of acarbose is modified upon binding, presumably through a series of hydrolysis and transglycosylation reactions. The end result is a pseudo-pentasaccharide moiety that spans the active site region with its N-linked "glycosidic" bond positioned at the normal site of cleavage. Interestingly, the side chains of Glu233 and Asp300, along with a water molecule, are aligned about the inhibitor N-linked glycosidic bond in a manner suggesting that these might act individually or collectively in the role of acid/base catalyst in the reaction mechanism. Indeed, kinetic analyses show that substitution of the side chains of either Glu233 or Asp300 leads to as much as a $\sim 10^3$-fold decrease in catalytic activity. Structural analyses of the Asp300Asn variant of human pancreatic α-amylase and its complex with acarbose clearly demonstrate the importance of Asp300 to the mode of inhibitor binding.

In humans, α-amylase (α-1,4-glucan-4-glucanohydrolase, E.C. 3.2.1.1) is present in both salivary and pancreatic secretions and plays a key role in catalyzing the hydrolysis of α-(1,4)-glycosidic linkages in starch (Figure 1). Both of these human α-amylase isozymes are composed of 496 amino acids in a single polypeptide chain and bind essential chloride and calcium ions (*3*, *4*). These isozymes are encoded on chromosome 1 as part of a multigene family that is regulated so that the different isozymes are expressed solely in either the salivary glands or the pancreas (*5*). Study of the human α-amylase genes and comparisons of their sequences suggest the recent duplication of an ancestral pancreatic α-amylase gene, followed by the acquisition of salivary specificity (*6*). The overall primary sequences of the pancreatic and salivary α-amylases are highly homologous (*7*), and this is reflected by a correspondingly high level of structural similarity (*2*, *8*).

Physiologically, the digestion of starch by α-amylase occurs in several stages in humans, with the salivary enzyme providing an initial partial cleavage into shorter oligomers (*9*). Once this partially digested material reaches the gut, it is then extensively hydrolyzed into smaller oligosaccharides by the α-amylase isozyme synthesized in the pancreas and excreted into the lumen. The resultant mixture of oligosaccharides then passes through the mucous layer of the brush border membrane, where additional α-glucosidases degrade it to glucose, which then enters the blood stream by means of a specific transport system. Inhibitors of pancreatic α-amylase and of the brush border glucosidase have proven useful in controlling postprandial blood glucose levels through slowing of the digestion of starch and related oligosaccharides (*10*−*15*). Indeed the naturally occurring inhibitor acarbose, originally isolated from *Streptomyces*, has been particularly valuable in this regard and has been studied in the treatment of diabetes (*9*, *16*). Acarbose is a pseudo-tetrasaccharide consisting of a polyhydroxylated aminocyclohexene derivative (valienamine) linked via its nitrogen atom to a 6-deoxyglucose, which is itself α-1,4-linked to a

[†] This work was funded by the Medical Research Council of Canada (MRC). G.S. is the recipient of an NSERC Postgraduate Scholarship. E.H.R. is the recipient of a MRC Studentship. C.M.O. is funded by a Clinician Scientist Award from the MRC.

[‡] Coordinates for the structures described in this work have been deposited in the Protein Data Bank (*1*) (accession numbers 1cpu, 2cpu, and 3cpu).

* To whom correspondence should be addressed. Phone: (604) 822-5216. Fax: (604) 822-5227. E-mail: brayer@laue.biochem.ubc.ca.

[§] Department of Biochemistry and Molecular Biology.

[||] Department of Chemistry.

[⊥] Department of Oral Biological and Medical Sciences.

10.1021/bi9921182 CCC: $19.00
Published on Web 03/30/2000

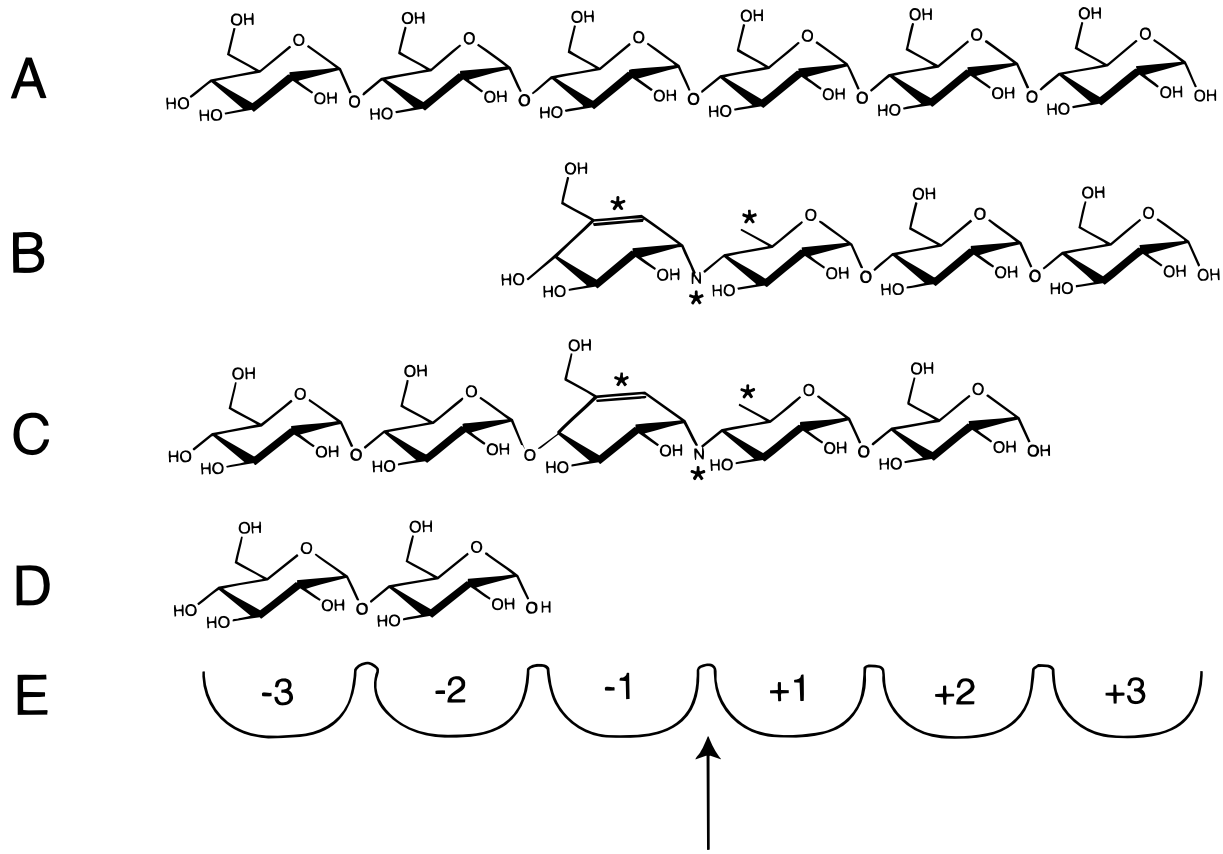

FIGURE 1: Schematic representations of (A) a portion of the normal polymeric starch substrate of human pancreatic α-amylase, (B) the chemical structure of acarbose, a potent inhibitor of this enzyme, (C) the rearranged structure of acarbose bound to the surface of human pancreatic α-amylase, (D) that portion of acarbose observed in a complex with the D300N variant protein, and (E) the convention used for designating substrate binding subsites in the active site of α-amylase. As indicated by the arrow, normal substrate cleavage takes place between the −1 and +1 subsites. Asterisks have been used to indicate the unique features of the pseudo-disaccharide unit of acarbose, which include a distorted unsaturated ring species, a methyl group in place of an exocyclic hydroxymethyl group, and an N-linked glycosidic bond.

maltose moiety (Figure 1). The strong inhibition of amylases by acarbose (K_i typically micromolar) is attributed both to the partial planarity of valienamine, which likely mimics the flattened ring of glucose at the oxocarbenium ion-like transition state (vide infra) during starch cleavage, and to the presence of strong electrostatic interactions between the carboxyl groups at the active site and the protonated nitrogen of the inhibitor.

Human pancreatic α-amylase belongs to family 13 of the sequence-related groupings assembled for glycosidases and glycosyl transferases (*17*, *18*). Despite low overall amino acid sequence homology within this family, short regions of highly conserved residues are present and structural studies have demonstrated that members of this family indeed have similar 3-dimensional structures (*2*, *19*). Overall, these family 13 enzymes are found to contain a characteristic $(\beta/\alpha)_8$-barrel catalytic domain and a variable number of other domains. HPA[1] consists of three structural domains, the largest of which, domain A, forms the eight-stranded parallel β-barrel on which are located the three putative active site residues Asp197, Glu233, and Asp300, as well as the chloride binding site (*2*). Domain B forms a calcium binding site next to the wall of the β-barrel of domain A, while domain C is only loosely associated with the other two domains and is of unknown function. Comparison of the structure of HPA with that of the closely related porcine enzyme (*20*, *21*) has revealed four regions of polypeptide chain with significantly different conformations. At least two of these regions occur in the vicinity of the active site and likely play a role in substrate binding and cleavage (*2*).

In common with other family 13 enzymes, HPA is believed to catalyze the hydrolysis of starch via a double-displacement mechanism involving the formation and hydrolysis of a covalent β-glycosyl enzyme intermediate as shown in Figure 2. Formation of this intermediate involves attack at the sugar anomeric center by a nucleophilic amino acid, most likely Asp197 by analogy with other family 13 enzyme sequences. This is assisted by general-acid catalysis provided by one or both of the other two active site carboxylic acids (Glu233 or Asp300). The covalent glycosyl enzyme intermediate then undergoes general-base-catalyzed hydrolysis via attack of water at the anomeric center, again assisted by one or both of the carboxyl groups of Glu233 or Asp300. As illustrated in Figure 2 this proposed mechanism is believed to proceed via oxocarbenium ion-like transition states.

To gain further insight into the catalytic mechanism of human pancreatic α-amylase and the substrate binding

[1] Abbreviations and Conventions: HPA, human pancreatic α-amylase; PPA, porcine pancreatic α-amylase; TAKA, *Aspergillus oryzae* α-amylase; amino acid numbering is according to a sequence alignment of HPA (*2*).

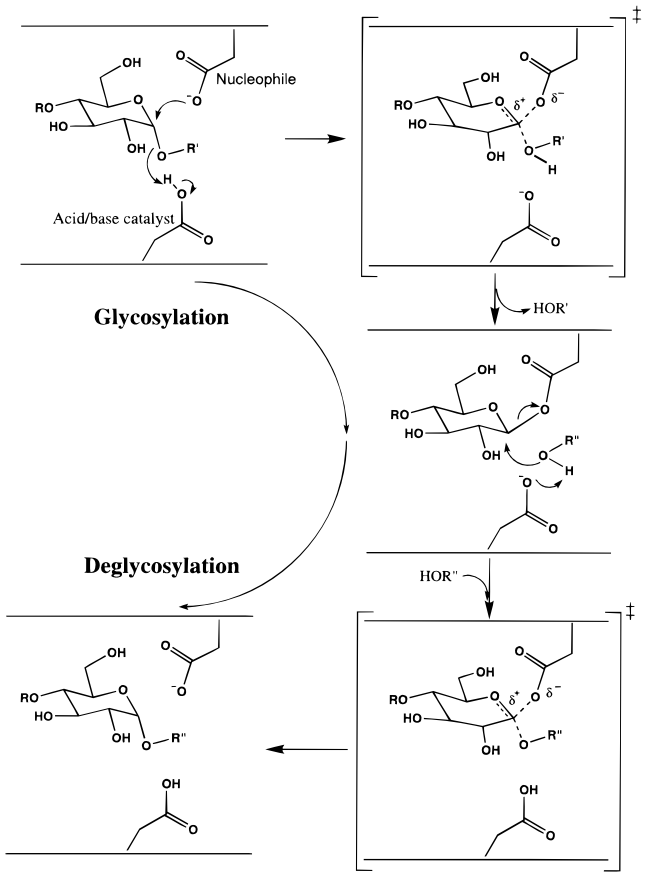

FIGURE 2: Schematic representation of the proposed catalytic mechanism of α-amylase. The nucleophile in this process is believed to be the side chain of Asp197 on the basis of analogy with other family 13 enzymes and on the basis of the results of kinetic analyses of variant enzymes. The identity of the acid/base catalyst(s) remains uncertain but most likely involves either, or perhaps both, of the side chains of Glu233 and Asp300. R″ in this case can represent either a hydrogen of a water molecule to give a cleavage reaction or alternatively some other sugar residue, which in this case would lead to a transglycosylation reaction.

subsites that facilitate its function, we have measured kinetic parameters for the hydrolysis of two separate series of substrates by the wild-type enzyme, as well as its dissociation constant for the pharmacologically applied inhibitor acarbose. Additional kinetic studies have been completed for HPA variants. A further element of these studies involved the determinations of the three-dimensional structures of the complexes formed by acarbose with the wild-type and D300N human pancreatic α-amylases. From past work, few substrate cleavage data are available for HPA, and in terms of acarbose inhibition of mammalian α-amylases, only the complex with the porcine enzyme has been studied in detail (*20*, *22*). Given the significant differences present between the structures of human and porcine pancreatic α-amylases (*2*), it is necessary to study substrate binding and acarbose inhibition directly with human α-amylase to facilitate our understanding of this enzyme's role in human metabolism. Such data are essential in the interpretation of clinical results and in the optimal design of improved inhibitory pharmaceutical agents to be used in therapeutic applications. The results of our current studies serve to delineate many aspects of the structure−function relationships in play between catalytic elements in the substrate binding cleft of human pancreatic α-amylase.

EXPERIMENTAL PROCEDURES

Substrates and Inhibitors. Malto-oligosaccharides were obtained from Boehringer-Mannheim. Buffer chemicals and other substrates were obtained from Sigma Chemical Co. unless otherwise stated. Acarbose was a generous gift of Miles Inc. (now Bayer). α-Glucosyl fluoride and α-maltosyl fluoride were synthesized following published procedures (*23*). Both 4-deoxy-α-maltosyl fluoride and 4-deoxy-α-maltotriosyl fluoride were synthesized according to previously published protocols (*24*). α-Maltotriosyl fluoride was synthesized according to the following procedure. An alternative approach is that of Junnneman et al. (*25*).

(a) 2,3,6,2′,3′,6′,2″,3″,4″,6″-Undeca-O-acetylmaltotriose. Maltotriose per-*O*-acetate (0.75 g, 0.78 mmol) was dissolved in dimethyl formamide (4 mL) and reacted with hydrazine acetate (0.10 mg, 1.09 mmol) at 50 °C for 25 min. Ethyl acetate was then added, and the solution was washed with water, saturated (satd) $NaHCO_3$ solution, and water and dried ($MgSO_4$). Evaporation in vacuo followed by flash chromatography (2:1 EtOAc−hexanes) (*26*) yielded the hemiacetal (0.41 g, 57%).

(2) 2,3,6,2′,3′,6′,2″,3″,4″,6″-Undeca-O-acetyl-α-maltotriosyl Fluoride. The protected hemiacetal prepared above (0.147 g, 0.16 mmol) was dissolved in dry CH_2Cl_2 (3 mL) and fluorinated using diethylaminosulfur trifluoride (24 mL, 0.20 mmol). Flash chromatography (2:1 ethyl acetate−hexanes) afforded mainly the *β*-fluoride. ^{19}F NMR ($CDCl_3$): δ −132.1 (*β*-F), −149.2 (α-F). To the syrup (0.11 g, 0.12 mmol) was added HF·pyridine (0.10 mL, 3.5 mmol) at −78 °C in a plastic vial, and the reaction was allowed to stir under a blanket of N_2 for 15 min, while the cooling bath was removed. Ether was added and the mixture washed with water, saturated aqueous $NaHCO_3$ solution, and water and dried ($MgSO_4$). Evaporation in vacuo followed by flash chromatography (ether) yielded the protected fluoride (77 mg, 70%) as a colorless gum. ^{19}F NMR ($CDCl_3$): δ −149.2 (dd, $J_{F1,1}$ 53.2 Hz, $J_{F1,2}$ 3.7 Hz, F-1).

(3) α*-Maltotriosyl Fluoride.* The per-*O*-acetylated maltotriosyl fluoride (1.5 g, 1.59 mmol) was deprotected with sodium methoxide according to previously published procedures (*27*). Flash chromatography (5:2:1 ethyl acetate−methanol−water) afforded pure α-maltotriosyl fluoride (0.6 g, 74%) as a colorless gum. ^1H NMR (D_2O): δ 5.67 (dd, 1 H, $J_{1,F1}$ 53.5 Hz, $J_{1,2}$ 2.7 Hz, H-1), 5.39 (d, 1 H, $J_{1′,2′}$ 3.9 Hz, H-1′), 5.36 (d, 1 H, $J_{1″,2″}$ 3.8 Hz, H-1″). ^{19}F NMR (D_2O): δ −150.4 (dd, $J_{F1,1}$ 53.6 Hz, $J_{F1,2}$ 26.3 Hz, F-1). Anal. Calcd for $C_{18}H_{31}FO_{15}·H_2O$: C, 41.22; H, 6.34. Found: C, 41.12; H, 6.52.

Human α*-Amylase Expression and Purification.* The wild-type enzyme from human pancreas was purified as described previously (*28*). The recombinant wild-type enzyme was expressed and isolated from *Pichia pastoris* cells (*29*). For the recombinant enzyme, cultures were incubated in BMGY medium (1% yeast extract, 2% peptone, 1% yeast nitrogen base, 1% glycerol, 100 mM potassium phosphate, pH 6.0) at 30 °C for 1 day. After 5-fold concentration by centrifugation (5 min, 5000*g*) expression was induced by using BMMY medium (1% yeast extract, 2% peptone, 1% yeast nitrogen base, 0.5% MeOH, 100 mM potassium phosphate, pH 6.0). Following 2 days of expression at 30 °C, with batchwise addition of 0.5% MeOH every 12 h, the *Pichia* cells were

removed by centrifugation (10 min, 5000*g*), leaving the secreted α-amylase in the supernatant.

Purification of this recombinant amylase proceeded with slow addition of cold EtOH with stirring at 4 °C until the supernatant contained 40% EtOH. This solution was allowed to stir for 1 h at 4 °C before centrifugation (12000*g*, 20 min, 4 °C). Glycogen (20 mg/mL) was added to the supernatant over a period of 5 min such that 1 mg of glycogen per 100 units of activity, as measured by a saccharogenic assay, was added. This solution was stirred for an additional 10 min at 4 °C before centrifugation (13000*g*, 5 min, 4 °C). The resulting small white pellet was dissolved in 30 mL of 20 mM phosphate buffer containing 25 mM NaCl, pH 6.9. The solution was left overnight at room temperature to allow complete digestion of the glycogen. The digested sample was dialyzed against 100 mM potassium phosphate (pH 7.4) at room temperature overnight. Following dialysis, the amylase solution was adjusted to 0.5 M NaCl and loaded onto a column (3 cm × 2 cm) of Phenyl-Sepharose CL-4B (Pharmacia) equilibrated in 100 mM phosphate buffer (pH 7.4). The bound protein was eluted with distilled water and concentrated to >2 mg/mL using a stirred-cell concentrator (Amicon). Deglycosylation of the secreted enzyme was performed by adding 10 μL of a 0.5 U/μL solution of a endoglycosidase F-cellulose binding domain fusion protein (*29*) to a solution of purified α-amylase (20 mL, 2 mg/mL, 25 mM NaCl, 50 mM phosphate buffer at pH 7.4). This solution was incubated at 37 °C for 4 h or at room temperature overnight. Deglycosylation was confirmed by SDS−PAGE before cellulose (0.5 g) was added to the solution. This suspension was gently mixed for 5 min before centrifugation (3500*g*, 5 min). The supernatant contained essentially pure deglycosylated α-amylase. This product was then subjected to ion exchange chromatography on a column (2 cm × 1 cm) of Q-Sepharose (Pharmacia) equilibrated in 20 mM phosphate buffer (pH 6.9) containing 25 mM NaCl.

Mutagenesis and Variant Protein Preparation. All commercially available vectors were acquired from Invitrogen (Carlsbad, CA). To perform site-directed mutagenesis in *E. coli* by the method of Kunkel et al. (*30*), the unique shuttle vector pHICL-AMY was constructed. This vector was designed to contain an F1 origin and the α-factor secretion sequence (as in pPIC9), which is thought to be more efficient than the PHO1 secretion sequence (as in pHIL-S1) (Invitrogen, Carlsbad, CA). This procedure involved the digestion of the vector pHIL-S1 (which contains a PHO1 secretion sequence and an F1 origin) with *Sac*1/*Sal*1, giving two fragments of 2949 and 5560 bp, which could be readily gel purified. The vector pPIC9-AMY (which contains the α-factor secretion sequence and the AMY insert) was digested with *Sac*1, *Sal*1, *Sca*1, *Sph*1, and *Dra*III. The resulting 5040 bp fragment was easily gel purified from the smaller DNA fragments of the other half of the vector. Ligation of two of the gel-purified fragments yielded the desired unique vector pHICL-AMY, which contained both the F1 origin and the α-factor secretion sequence of the parent vectors. Mutagenesis was performed using the single-stranded dUTP-DNA method (*30*). A 60−80% mutation rate was commonly achieved. Mutant cDNAs were fully sequenced (*31*) to confirm the fidelity of the reaction. The mutant cDNA was then linearized using *Sac*1 and transformed by electroporation (Invitrogen, Carlsbad, CA).

Expression of variant forms of HPA in *P. pastoris* was carried out as described for the wild-type form of this enzyme. However, subsequent purification protocols for variant enzymes were modified since saccharogenic assays indicated that these had very low activity; thus, affinity precipitation with glycogen could not be used as a method of purification. Instead, the culture medium was adjusted to pH 7.0 with NaOH and filtered through a 0.45 μm membrane (Gelman). The filtrate was then loaded onto a Phenyl-Sepharose CL-4B column (3 cm × 2 cm) equilibrated in 100 mM potassium phosphate buffer at pH 7.0. After being washed with 100 mM phosphate buffer (pH 7.0), the bound protein was eluted with distilled water. The eluant was concentrated using an Amicon stirred cell concentrator, and the buffer was adjusted to 20 mM potassium phosphate (pH 6.9) containing 25 mM NaCl. At this point, the variant protein was deglycosylated using endoglycosidase F-cellulose binding domain fusion protein and further subjected to ion exchange chromatography as described for the wild-type protein. The variant α-amylase obtained from the flow-through was >99% pure as determined by SDS−PAGE.

Kinetic Assays. General Procedures. Values of k_{cat} and K_m were determined by measuring rates at 5−8 different concentrations of the substrate ranging from 0.3 to 5 times the K_m value ultimately determined, using the assays described below. Values of K_m and k_{cat} were calculated by fitting the data to the Michaelis−Menten equation by weighted nonlinear regression using the computer program Grafit (*32*).

Kinetic Assays. Malto-oligosaccharides. HPLC analyses were performed on instrumentation from Waters, comprising the following: model 712 WISP autosampler, model 410 differential refractive index detector, a Novapak C_{18} Guard-Pak precolumn, and an analytical Dextropak column (100 × 8 mm; water as eluent). A SIM interface module was used to allow the data to be collected on the computer using the Baseline 810 chromatography workstation. Chromatographs were exported from the workstation as ASCII data files to the computer program Grafit (*32*) for printing.

Product distributions were determined by HPLC analysis. To separate solutions (160 μL) of maltotetraose (0.5 mM), maltopentaose (0.5 mM), maltohexaose (0.5 mM), and maltoheptaose (0.5 mM) in 50 mM sodium phosphate buffer (pH 6.8) were added aliquots of α-amylase (21, 0.84, 2.1, and 0.42 μg, respectively). Each reaction mixture was injected onto the HPLC 1 min after enzyme was added, and the product distribution was determined. The assignment of peaks was achieved by comparing retention times with the standard malto-oligosaccharides, glucose to maltoheptaose. The amount of each product formed was determined by measuring the area under the peak as determined by the Baseline 810 chromatography workstation. The peak areas were converted to concentrations by determining standard curves for each of the standards, maltose, maltotriose, and maltotetraose. The cleavage sites were also determined from the product distribution experiments by observing which oligosaccharides were released as their pure α-anomers.

The kinetic constants were determined by HPLC analysis using a Dextropak column. Solutions of maltotriose to maltoheptaose, at five different concentrations, were incubated with α-amylase at 30 °C in 20 mM sodium phosphate, 25 mM sodium chloride buffer (pH 6.9). Aliquots of each

Table 1: Summary of Diffraction Data Collection Values

parameters	wild-type/ acarbose complex	D300N variant	D300N variant/acarbose complex
space group	$P2_12_12_1$	$P2_12_12_1$	$P2_12_12_1$
cell dimensions (Å)			
a	52.95	52.80	52.91
b	68.79	68.77	75.39
c	131.93	131.36	136.12
no. of measurements	157 746	170 318	119 912
no. of unique reflns	33 610	31 970	31 361
mean $I/\sigma I$[a]	17.9 (10.3)	13.0 (5.8)	9.7 (3.2)
multiplicity[a]	4.7 (2.8)	4.5 (3.5)	3.8 (1.6)
merging R factor (%)[b]	3.7	8.1	7.9
max resolution (Å)	2.0	2.0	2.0

[a] Values in parentheses are for the highest resolution shell (2.07−2.00 Å resolution). [b] $R_{merge} = \sum_{hkl}\sum_{i=0}^{n}|I_i - \bar{I}_{hkl}|/\sum_{hkl}\sum_{i=0}^{n}I_{ihkl}$.

Table 2: Summary of Structure Refinement Statistics

parameters	wild-type/ acarbose complex	D300N variant	D300N variant/ acarbose complex
no. of reflns	31 856	31 368	30 916
resolution range (Å)	8.0−2.0	8.0−2.0	8.0−2.0
completeness within range (%)[a]	93.8 (91.2)	96.1 (95.9)	83.4 (80.3)
no. of protein atoms	3946	3946	3946
no. of solvent atoms	261	177	233
avg thermal factors (Å^2)			
protein atoms	16.3	15.1	16.2
solvent atoms	36.4	31.7	30.4
final refinement *R* factor (%)[b]	17.0	16.7	17.9
stereochemistry		rms deviations	
bonds (Å)	0.008	0.010	0.010
angles (deg)	1.265	1.308	1.330

[a] Values in parentheses are for the highest resolution shell (2.07−2.0 Å resolution). [b] *R* factor $= \sum_{hkl}|F_o - F_c|/\sum_{hkl}|F_o|$.

reaction mixture were removed at time intervals, boiled for 2 min to denature the enzyme, and injected onto the HPLC column for analysis. Initial rates were determined by monitoring the increase in concentration of a particular product over time. The kinetic constants, K_m and k_{cat}, were thus determined as described above.

Kinetic Assays. Malto-oligosaccharyl Fluorides. Reaction rates were determined by monitoring the release of fluoride using a fluoride ion electrode as described previously (*33*). The assays were performed at 30 °C in 20 mM sodium phosphate buffer (pH 6.9) containing 25 mM NaCl. Stock enzyme (5 μL of 50 nM wild-type enzyme, or 10 μL of 3.6 μM variant enzyme) was added to glass cells containing various concentrations of the glycosyl fluoride in a total assay volume of 300 μL. Controls were performed to compensate for the spontaneous hydrolysis of the substrates. The fluoride released after hydrolysis was detected using an Orion 96-09 combination fluoride ion electrode coupled to a Fischer Accumet 925 pH/ion meter and interfaced with a Pentium 133 MHz personal computer.

Structure Determinations. Crystals of the recombinant wild-type and D300N variant proteins were grown at room temperature using the hanging drop vapor diffusion method. The reservoir solution contained 60% 2-methylpentane-2,4-diol with 100 mM cacodylate at pH 7.5, and the hanging drops consisted of 5 μL of protein solution (2 mg/mL) mixed with 5 μL of reservoir solution. Diffraction-quality crystals appeared over the period of a month. Crystals of complexed recombinant wild-type and D300N HPA were prepared by immersing newly grown crystals in a stock solution containing 200 mM acarbose for a period of 4 h.

Diffraction data for the wild-type HPA/acarbose complex, the D300N variant, and the D300N/acarbose complex, were collected on a Rigaku R-AXIS IIC imaging plate area detector system using Cu Kα radiation supplied by a Rigaku RU300 rotating anode generator operating at 50 kV and 100 mA. A total of 100 (0.9° oscillation), 90 (1.0° oscillation), and 120 (0.8° oscillation) data frames were collected, respectively. All data frames were exposed for 30 min. The intensity data were then integrated, scaled, and reduced to structure factor amplitudes with the HKL suite of programs (*34*). Data collection statistics are provided in Table 1. Data collection and structure solution methods used for uncomplexed recombinant wild-type HPA have been described previously (*29*). The results of diffraction data collections showed that crystals of the D300N HPA variant protein and the recombinant wild-type HPA/acarbose complex were isomorphous with those of the recombinant wild-type protein. Therefore, the structural model of recombinant wild-type HPA (with residue 300 truncated to an alanine for the D300N variant structure) was used as the starting refinement model for these proteins. However, since space group parameters determined for the D300N variant/acarbose complex were not isomorphous with those of recombinant wild-type HPA, a molecular replacement approach was taken to the solution of this structure using the AMoRe package (*35*). In this process, the recombinant wild-type HPA structure was used as a search model. A rotation function search with data from 8 to 4 Å resolution resulted in a single significant peak having a height of 7.5σ and a correlation coefficient of 29.4. This rotation function solution was then used in the translation function search. The best translation function solution had a correlation coefficient of 85.1. Combining the best rotation and translation function results produced a conventional crystallographic *R* factor of 25.1%.

Additional refinement of all three structural models was accomplished with X-PLOR (*36*) software wherein cycles of simulated annealing and positional and thermal *B* refinements were alternated with manual model rebuilding with O (*37*). The complete polypeptide chain of all three refinement models was examined periodically during this process with $F_o - F_c$, $2F_o - F_c$, and fragment-deleted difference electron density maps. During such examinations, the positions of the remaining atoms of N300 in the D300N variant and D300N/acarbose complex structures were determined, bound acarbose (or portions thereof) was positioned, solvent molecule peaks were assigned, and an *N*-acetylglucosamine moiety was built into observed electron density extending from the side chain of Asn461 in the wild-type/acarbose complex structure. Neither the D300N variant nor the D300N/acarbose complex structure showed any evidence of glycosylation at Asn461. The validity of solvent molecules was assessed on the basis of both hydrogen-bonding potential to protein atoms and the refinement of a thermal factor of <75 Å^2. Final refinement statistics for each structure determination are detailed in Table 2. Coordinate error, as estimated from a Luzzati plot (*38*), is 0.20 Å for the HPA/acarbose complex, 0.19 Å for the D300N HPA/acarbose complex, and 0.19 Å for D300N HPA.

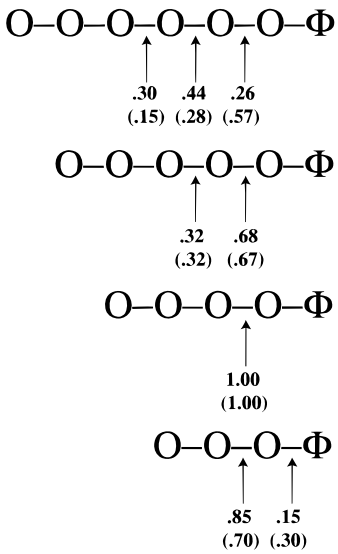

FIGURE 3: "Action pattern" for HPA-catalyzed hydrolysis of maltotetraose, maltopentaose, maltohexaose, and maltoheptaose and the ratio of occurrence of different cleavage points in each substrate (−, α-(1,4) glycosidic linkage; Φ, reducing sugar; O, nonreducing sugar). Numbers in parentheses are for PPA (*47*).

RESULTS AND DISCUSSION

(a) Cleavage Action Patterns with Malto-oligosaccharides. The sites of cleavage for each oligosaccharide, and the ratios of products formed, were determined by monitoring the hydrolysis of each oligosaccharide at a single concentration by means of HPLC analysis using a Dextropak column as described in the Experimental Procedures. Use of this approach allows the site of cleavage to be determined without needing to specifically end-label each oligosaccharide since the Dextropak column separates the two anomers of malto-oligosaccharides containing three or more glucose residues. Therefore, since the enzyme is known to cleave with retention of anomeric configuration, the oligosaccharide detected as the single α-anomer must derive from the nonreducing terminus of the oligosaccharide substrate and that released as the α/β mixture must derive from the reducing terminus. Product ratios were determined from peak areas. The results obtained from this analysis are shown in Figure 3, in which arrows indicate cleavage position and the numbers reflect percent cleavage observed at each point. Such numbers should be directly proportional to the relative k_{cat}/K_m values for cleavage at each position.

Two productive binding modes are seen for maltotetraose, the preferred cleavage mode being the symmetrical one in which the −2 to +2 subsites are filled (Figure 1). Two productive binding modes were also observed for cleavage of maltohexaose, the preferred cleavage mode being that in which the −4 to +2 subsites are occupied and not the symmetrical (−3 to +3) mode. Maltopentaose is the only substrate to be cleaved at only one site, indicating a single productive binding mode in which the −3 to +2 subsites are filled. Interestingly, in each of these cases the preferred binding/cleavage mode is one in which a maltose residue serves as the leaving group, suggesting that a minimum of two residues is required in the aglycon (+n) site for optimal cleavage rates. The preference for three sugars in the glycon (−n) sites thus suggests that a total of five subsites make up the active site. Results with maltoheptaose, as might be expected, are more complex, with three roughly equivalent productive binding modes. These results are in general agreement with those obtained for the porcine pancreatic enzyme since a total of five subsites was proposed in that case. However, the results with the longer oligosaccharides do suggest significant differences in active site architecture.

(b) Michaelis−Menten Parameters for Hydrolysis of Malto-oligosaccharides. Values of k_{cat} and K_m for hydrolysis of each of these substrates in each mode were determined by careful monitoring of rates of release of each product via HPLC analysis, using a series of substrate concentrations. These are shown in Table 3. Comparison with the data in Figure 3 reveals that the k_{cat}/K_m values for the different cleavage processes agree reasonably well with expectations from the action patterns described above. However, more importantly these data provide excellent insights into the relative rates of hydrolysis with the different oligosaccharide substrates. Thus, maltotriose is a very poor substrate with by far the lowest k_{cat} and highest K_m of all the substrates tested. Maltotetraose is a much better substrate, binding productively in two ways, with that in which both the +1 and +2 subsites are filled being preferred. Maltopentaose is a yet better substrate in terms of k_{cat} and k_{cat}/K_m, but with a very similar K_m value. Maltohexaose has two cleavage modes with very similar k_{cat} values. However, the k_{cat}/K_m values concur with the finding from the action patterns that the mode yielding G4 and G2 as products is dominant, possibly indicating the existence of an additional, lower affinity subsite at the −4 position. Indeed, the highest k_{cat}/K_m value observed is that for maltoheptaose binding such that it fully fills the −4 to +3 subsites.

These results are very roughly comparable to those reported previously for the porcine enzyme (*39*) and reproduced in Table 3. However, some significant differences are noted. For example, the human enzyme cleaves shorter oligosaccharides with higher k_{cat} values than does the porcine enzyme, but with higher K_m values also, resulting in very similar k_{cat}/K_m values. Porcine enzyme K_m values for the longer oligosaccharides are similar to each other, and to values for the human enzyme, but k_{cat} values are apparently significantly higher, although the separate modes of cleavage were not evaluated.

(c) Michaelis−Menten Parameters for the Cleavage of Malto-oligosaccharyl Fluorides. Glycosyl fluorides have been shown previously to function as substrates for amylases (*40*), cleaving via both hydrolysis and transglycosylation. Kinetic parameters for their hydrolysis by the human enzyme would therefore be of value since they would provide insight into binding in the −n sites without interference from the +n sites as the good leaving group ability of fluoride replaces the need for aglycon interactions. Kinetic parameters for the cleavage of α-maltosyl fluoride and α-maltotriosyl fluoride are provided in Table 4, along with values for some analogues. HPLC analysis of product mixtures resulting from partial cleavage of these substrates revealed that both transglycosylation and hydrolysis were occurring (data not shown). Cleavage of α-maltosyl fluoride yielded both maltose and maltotetraose, while cleavage of α-maltotriosyl fluoride yielded a mixture of oligosaccharides including maltotriose, maltotetraose, maltohexaosyl fluoride, and maltosyl fluoride. Presumably transglycosylation yielded maltohexaosyl fluoride first, which then cleaved to yield

Table 3: Kinetic Evaluation of Malto-oligosaccharides as Substrates for Human and Porcine Pancreatic α-Amylases

enzyme	substrate	products	K_m (mM)	k_{cat} (s^{-1})	k_{cat}/K_m (s^{-1} mM^{-1})	ref
HPA	maltotriose	G2 + G1	10.9 ± 1.9	2.6 ± 0.2	0.24 ± 0.06	*a*
HPA	maltotetraose	G2 + G2	0.86 ± 0.11	100 ± 4	116 ± 19	*a*
HPA	maltotetraose	G3 + G1	0.51 ± 0.12	17.4 ± 1.2	27.5 ± 8.4	*a*
HPA	maltopentaose	G3 + G2	1.0 ± 0.1	408 ± 17	408 ± 57	*a*
HPA	maltohexaose	G4 + G2	0.40 ± 0.09	167 ± 9	418 ± 117	*a*
HPA	maltohexaose	G3 + G3	1.1 ± 0.4	150 ± 21	136 ± 68	*a*
HPA	maltoheptaose	G4 + G3	0.74 ± 0.11	375 ± 16	507 ± 98	*a*
HPA	maltoheptaose	G5 + G2	0.70 ± 0.11	98.1 ± 5.4	140 ± 30	*a*
PPA	maltotriose	G2 + G1	0.5	0.13	0.27	*b*
PPA	maltotetraose	G2 + G2	0.7	79.1	110	*b*
PPA	maltotetraose	G3 + G1	0.7	38.9	54.0	*b*
PPA	maltopentaose	G3 + G2	1.08	1360	1260	*b*
PPA	maltohexaose	all rxns	0.62	1270	2050	*b*
PPA	maltoheptaose	all rxns	1.02	1250	1220	*b*

[a] This work. [b] From ref *39*.

Table 4: Kinetic Parameters for Wild-Type and Variant HPAs with Glycosyl Fluoride Substrates

enzyme	substrate[g]	K_m (mM)	k_{cat} (s^{-1})	k_{cat}/K_m (s^{-1} mM^{-1})	fold decrease in k_{cat}/K_m
HPA-gly[a]	αG3F	0.34 ± 0.038	280 ± 8.1	830 ± 120	1.0[c]
HPA-dgly[b]	αG3F	0.26 ± 0.023	215 ± 4.7	850 ± 93	0.98[c]
D197N	αG3F	1.1 ± 0.22	(7.3 ± 1.80) × 10^{-4}	(6.6 ± 0.56) × 10^{-4}	1 200 000[c]
E233Q	αG3F	0.085 ± 0.028	6.6 ± 0.75	77 ± 34	11[c]
D300N	αG3F	0.89 ± 0.098	0.15 ± 0.006	0.17 ± 0.025	4900[c]
HPA[e]	4DαG3F	0.49 ± 0.04	303 ± 8	618 ± 67	1.3[c]
HPA[f]	αG2F	4.5 ± 0.1	443 ± 5	98 ± 3	1.0[d]
HPA[e]	4DαG2F	9.1 ± 1.2	489 ± 27	54 ± 10	1.8[d]
HPA[f]	2FαG2F	4.7 ± 0.9	0.17 ± 0.02	0.04 ± 0.01	2450[d]

[a] HPA-gly = glycosylated HPA cloned and expressed in *P. pastoris*. [b] HPA-dgly = endoglycosidase F digested HPA-gly. [c] Relative to αG3F. [d] Relative to αG2F. [e] The enzyme used in these analyses was expressed and isolated from BHK cells as described in ref *29*. [f] The enzyme used in these analyses was isolated from pancreas (*2*). [g] Abbreviations used to designate substrates; αG3F, α-maltotriosyl fluoride; αG2F, α-maltosyl fluoride; 4DαG3F, 4″-deoxy-α-maltotriosyl fluoride; 4DαG2F, 4′-deoxy-α-maltosyl fluoride; 2FαG2F, 2-deoxy-2-fluoro-α-maltosyl fluoride.

maltotetraose and maltosyl fluoride, as would be predicted from the previous results. Maltotriose arises from hydrolysis of either maltotriosyl fluoride itself or maltohexaosyl fluoride.

The identity of the rate-limiting step (glycosylation or deglycosylation of the enzyme) is not clear from these results. However, some insight was obtained by kinetic analysis of substrates in which the nucleophilic 4-hydroxyl had been removed, thereby prohibiting the transglycosylation pathway. Kinetic parameters for hydrolysis of 4′-deoxymaltosyl fluoride and 4″-deoxymaltotriosyl fluoride are presented in Table 4. As can be seen, k_{cat} values for maltosyl fluoride and 4′-deoxymaltosyl fluoride are very similar, as are the values for maltotriosyl fluoride and its 4″-deoxy analogue. This implies that the same step is rate-limiting in the two cases. Since transglycosylation is a major pathway for cleavage of the unsubstituted glycosyl fluorides but is impossible for the 4-deoxy analogues, as confirmed by HPLC analysis of reaction mixtures, then it seems probable that the glycosylation step is rate-limiting in the two cases. No important interactions appear to be present at the 4-position as revealed by the fact that K_m values for the two maltotriose analogues were very similar, and that for 4′ -deoxymaltosyl fluoride was only slightly larger than that for maltosyl fluoride. This is not surprising given that this oxygen would ordinarily be involved in a glycosidic bond in the natural (starch) substrate. The k_{cat}/K_m values should reflect the glycosylation step since this parameter gives information on the first irreversible step. It is therefore gratifying to see that the k_{cat}/K_m value for maltotriosyl fluoride is approximately 4 times greater than that for maltosyl fluoride, this 4-fold increase as a consequence of filling the −3 site being identical to that seen in comparing k_{cat}/K_m values for cleavage of maltopentaose and maltotetraose when both are bound with the +1 and +2 sites filled.

Interestingly, quite different kinetic behavior was seen for the cleavage of α-glucosyl fluoride. The plot of reaction rate versus concentration of α-glucosyl fluoride was upward curving, and approximately fit by a quadratic function (data not shown). This suggests that 2 molecules of substrate are required in the rate-determining step of the reaction, most likely indicating that deglycosylation is now rate-limiting and that α-glucosyl fluoride must also bind in the adjacent site as acceptor. Product analysis by HPLC indeed confirmed the formation of oligosaccharide products.

A final analogue tested was 2-deoxy-2-fluoro-α-maltotriosyl fluoride. 2-Deoxy-2-fluoroglycosyl fluorides have been shown previously to function as excellent time-dependent inactivators of *β*-glycosidases, functioning via the accumulation of a relatively stable glycosyl enzyme intermediate (*41*). However, with α-glycosidases and α-glycosyl transferases they have tended to act rather as slow substrates for which the glycosylation step is rate-limiting (*42*). Consistent with this, no time-dependent inactivation was observed when 2-deoxy-2-fluoro-α-maltotriosyl fluoride was incubated with human amylase. However, analysis of reaction mixtures using a fluoride electrode revealed that the analogue was indeed functioning as a slow substrate, with a K_m value very similar to that of maltosyl fluoride and a k_{cat} value almost 3000-fold lower. Such large rate decreases are primarily a consequence of the inductive destabilization of the oxocarbenium ion-like transition state afforded by the electronegative fluorine substituent.

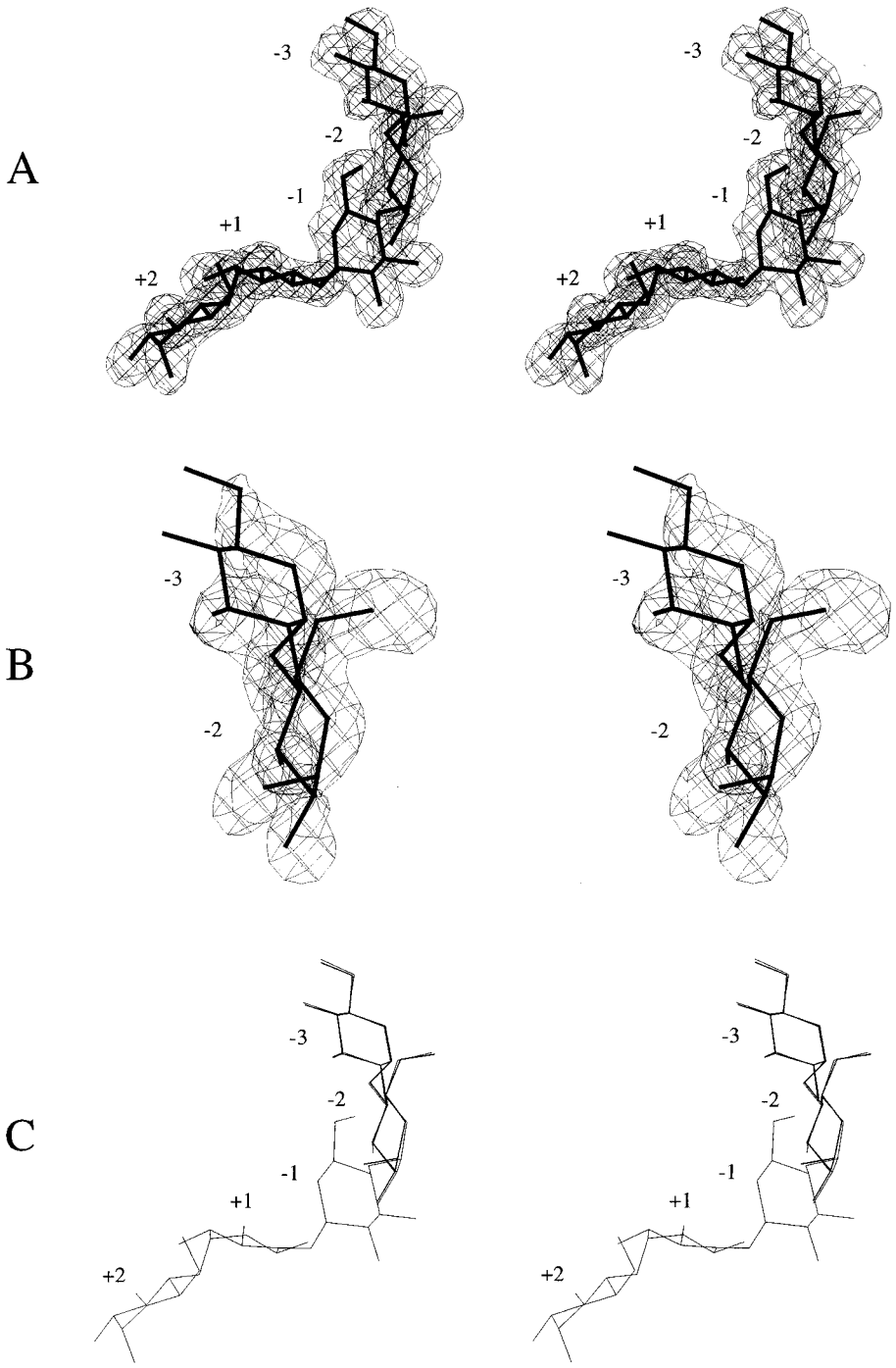

FIGURE 4: Stereo drawings of omit difference electron density maps showing (A) the bound conformation of modified acarbose in the active site of wild-type HPA and (B) the maltose unit that is visible in the related D300N/acarbose complex. These maps have been contoured at the 2.5σ level, and the final refined coordinates of inhibitor atoms are drawn (also see Figure 1). In (C) the active site placements for the acarbose inhibitor structures bound to wild-type and D300N HPA are overlaid for comparison.

(d) Structural Studies of the HPA/Acarbose Complex. Previous determinations of the essentially identical three-dimensional structures of natural and recombinant wild-type HPA have been presented (*2*, *29*). As shown in Figure 1, the inhibitor acarbose is found bound in the active site cleft of HPA and as part of the binding process undergoes significant chemical rearrangement, apparently the result of a series of hydrolysis and transglycosylation events. The end product is a pseudo-pentasaccharide centered in the region of the three catalytic carboxyl groups of Asp197, Glu233, and Asp300. Overall the modified inhibitor binds in subsites -3 through $+2$, corresponding to the five major binding subsites identified through kinetic results described herein.

The primary factors allowing for the unique identification of the five rings of the modified acarbose bound to HPA are illustrated in Figure 1, and hinge on the differences between the pseudo-disaccharide acarviosine unit of this inhibitor and maltose. The most prominent of these arises from the absence of the glucose 6-hydroxyl in the sugar portion of acarviosine, though care must be taken since this might be difficult to distinguish from a disordered hydroxyl group at this position. To minimize bias, in this identification

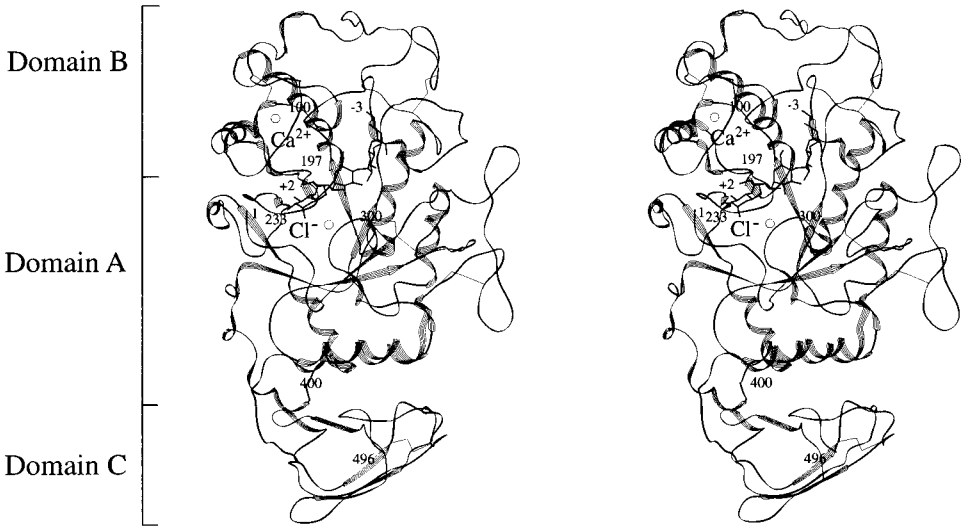

FIGURE 5: A stereo drawing showing the overall polypeptide chain fold of human pancreatic α-amylase. The relative positionings of the three structural domains present in this enzyme are indicated, along with the locations of the calcium and chloride binding sites. Domain A is composed of residues 1−99 and 169−404, domain B is composed of residues 100−168, and domain C is constructed from residues 405−496. The central feature of this structure is an eight-stranded parallel β-barrel that forms the bulk of domain A and contains the active site region. Also drawn is the placement of the modified form of acarbose that our studies have shown is bound in the active site cleft of HPA. The enzyme binding subsites −3 and +2, to which the ends of the bound inhibitor bind, have been labeled, as have the locations of various amino acids along the course of the polypeptide chain.

process the structure of the HPA/acarbose complex was initially refined without inhibitor atoms present. Upon convergence of the refinement of the enzyme portion of the complex, a difference electron density map was then used to interpret the structure and conformation of the bound and modified acarbose. Detailed analysis of this well-defined map and subsequent omit difference electron density maps clearly indicated the presence of five saccharide rings and showed that only one of these was missing an exocyclic hydroxyl group (Figure 4). This allowed for the assignment and positioning of the pseudo-disaccharide acarviosine unit of acarbose and provided confirmation that only one such unit was present.

Following placement of all five ring elements of the modified acarbose inhibitor, subsequent refinement of the full HPA/acarbose complex was carried out to completion. Inhibitor refinement was based on full occupancy for all atoms, and as Figure 4 shows, all elements of this molecule were exceptionally well resolved. This is also reflected in the average saccharide ring thermal factors of 15.0, 9.9, 9.2, 6.4, and 15.2 Å^2, for each of these bound in subsites −3 to +2, respectively. As Figure 5 illustrates, the modified acarbose inhibitor is tightly bound in the pronounced active site cleft that crosses the surface of HPA. The valienamine moiety, whose half-chair conformation may mimic that of the substrate at the reaction transition states, is found in binding subsite −1, with the 4-amino-4,6-dideoxyglucose moiety in subsite +1 (Figure 1). The strong inhibition by acarbose is believed to result from enhanced binding of the valienamine moiety, whose half-chair conformation may mimic substrate distortions present in catalytic transition states. The N-linked glycosidic bond is located at the position where normal substrate cleavage would occur and is most likely protonated under the conditions used. Within this complex, the inhibitor also makes direct contacts with the side chains of Asp197, Glu233, and Asp300.

A detailed stereo drawing of the active site of HPA illustrating the bound conformation of modified acarbose is shown in Figure 6. Extensive hydrophilic and hydrophobic interactions are formed between this inhibitor and the enzyme surface in each of the five binding subsites occupied. Figure 7 details the interactions formed, and Figure 8 shows a close-up view of the region directly about the N-linked glycosidic bond of the pseudo-disaccharide acarviosine unit of the inhibitor, along with the conformations of the nearby catalytic residues. Particularly prominent among the contacts observed is a hydrogen bond formed between the side chain of Asp300 and the N−H group that mimics the glycosidic bond that is normally cleaved by HPA. The same Asp300 side chain carboxyl oxygen atom involved in this interaction also forms a hydrogen bond to the 2-hydroxyl of the valienamine residue, as well as to a water molecule (Wat507) bound between this residue and the side chain of Glu233. The alternative carboxyl oxygen of Asp300 forms a hydrogen bond with the 3-hydroxyl group of the valienamine residue.

Together, the side chains of Asp300 and Glu233, as well as the water molecule jointly bonded between them, are arranged around the N−H glycosidic link as one might expect the acid/base catalyst of the proposed reaction scheme for HPA to be located (Figure 2). Note the closest approaches to this nitrogen atom for Asp300, Glu233, and Wat507, are 3.04, 2.87, and 4.03 Å, respectively. The importance of both Asp300 and Glu233 to catalytic activity is also clearly demonstrated in the kinetic results outlined in Table 4, which show substitution of either of these residues leads to as much as a $\sim 10^3$-fold decrease in enzymatic activity.

The observed conformations of Glu233 and Asp300 in the HPA/acarbose complex are similar to those seen previously in the acarbose complexes of porcine pancreatic α-amylase (*22*) and TAKA α-amylase (*43*). A comparison of the glycosidic bond angles and hydrogen bonds of these acarbose complexes is detailed in Table 5. These results are also reminiscent of interactions found in the complexes of another family 13 enzyme, the *Bacillus* cyclodextrin glucanotransferase, both in an enzyme/substrate Michaelis complex of a mutant form of the enzyme and also in the trapped covalent

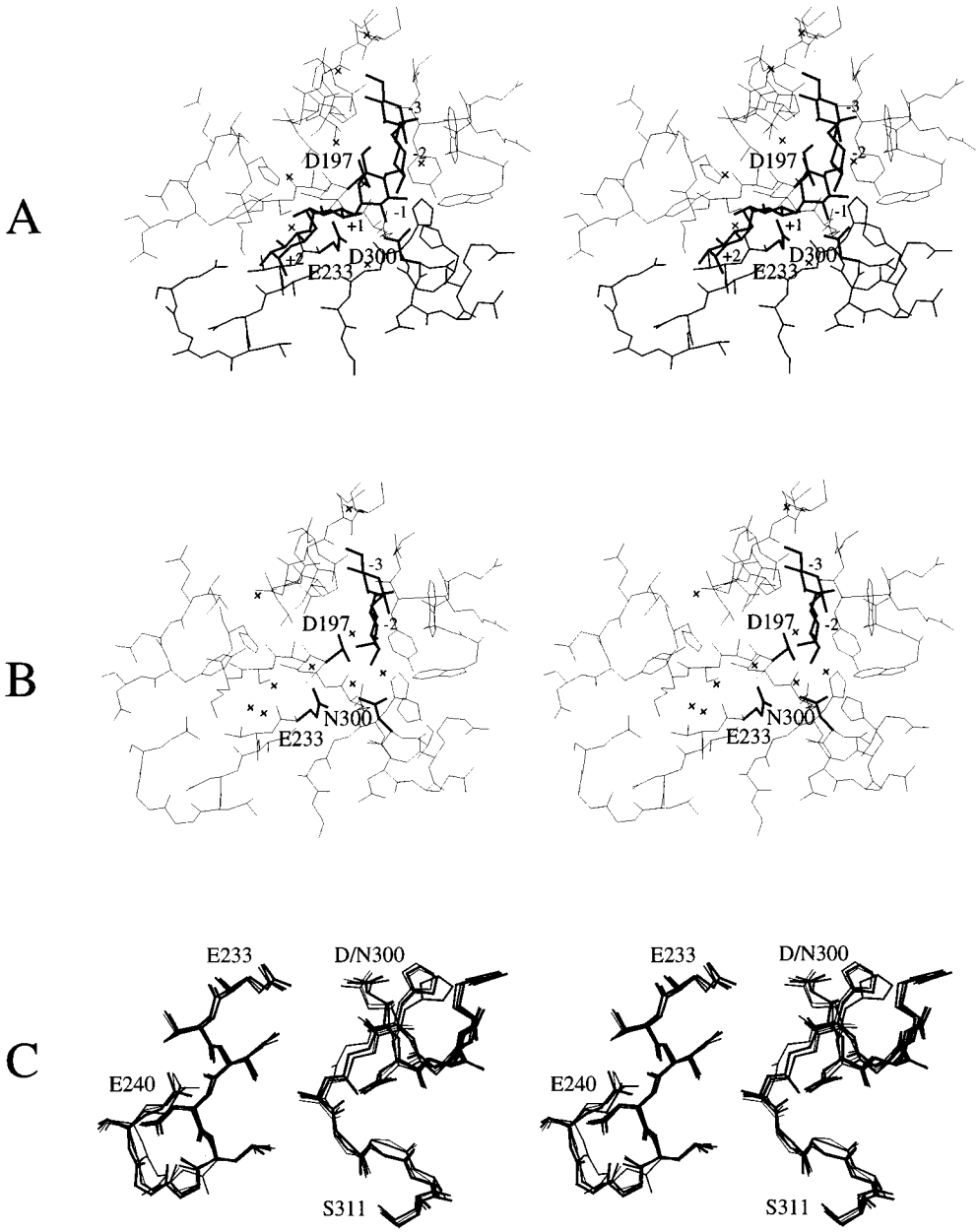

FIGURE 6: Stereo plots of the active site regions in the (A) wild-type/acarbose and (B) D300N variant/acarbose complex structures of human pancreatic α-amylase. The three active site residues believed to be directly involved in catalytic activity have been labeled, as have the subsite binding positions for each bound inhibitor ring. In (A) the two strands of polypeptide chain containing residues E233 and D300 have been drawn with darker lines. Water molecules are indicated with crosses. In (C) a stereo plot is presented of those portions of polypeptide chain most affected by inhibitor binding or the substitution of residue 300. Drawn from thinnest to thickest lines are the polypeptide chain conformations of the wild type, wild-type/acarbose complex, D300N variant, and D300N variant/acarbose complex.

Table 5: Observed Glycosidic Bond Angles and Hydrogen Bonds in Acarbose Complexes[a]

	φ (deg)			ψ (deg)			O2 − O3′ (Å)		
glycosidic linkage	HPA	PPA	TAKA	HPA	PPA	TAKA	HPA	PPA	TAKA
−3/−2	116	116	144	−111	−107	−106	2.83	2.72	2.88
−2/−1	88	89	121	−145	−150	−102			2.93
−1/+1	21	17	33	−148	−149	−151			
+1/+2	118	113	110	−110	−99	−120	2.68	2.84	2.71
+2/+3			121			−107			2.65

[a] HPA, human pancreatic α-amylase (*2*); PPA, porcine pancreatic α-amylase (*20*); TAKA, *A. oryzae* α-amylase (*43*).

intermediate (*44*). Of particular interest is the location of Asp328 in that structure (equivalent to Asp300 in HPA), which bridges the 2- and 3-hydroxyl groups in binding subsite −1 and appears to play a role in distortion of the substrate.

On the opposite side of the imino ether bond of the inhibitor, the side chain of Asp197 is found in a location where it could easily carry out a nucleophilic attack on the C1 carbon of the sugar ring bound in subsite −1 if a normal glucose unit was present (Figures 6 and 8). In the current

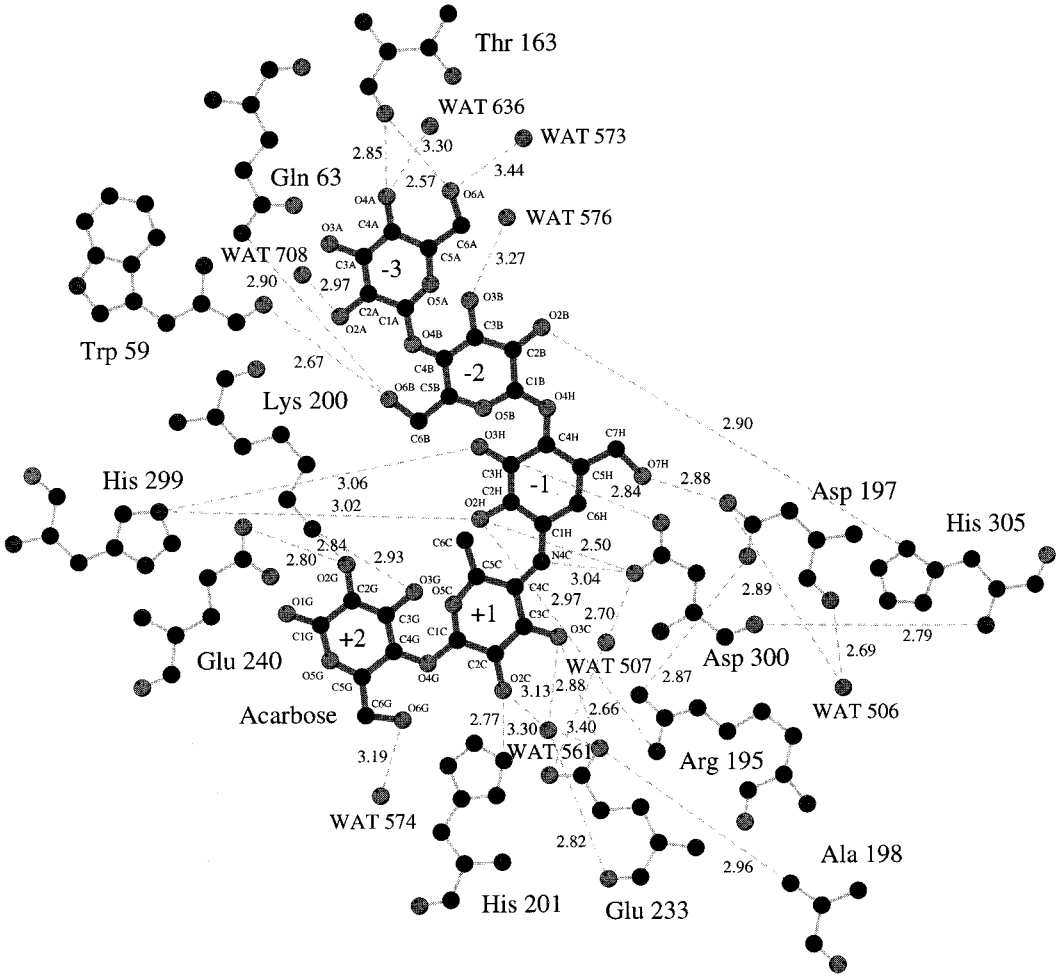

FIGURE 7: A diagrammatic illustration of the interactions formed by the modified form of acarbose bound in the active site of HPA. Active site substrate binding subsites have been labeled from −3 to +2 (Figure 1). For clarity, individual non-hydrogen atoms of the bound inhibitor are labeled. Hydrogen bond interactions are indicated with dashed lines, and the lengths of these are given in angstroms. This figure was generated with the assistance of the programs HBPLUS (*48*) and Ligplot (*49*).

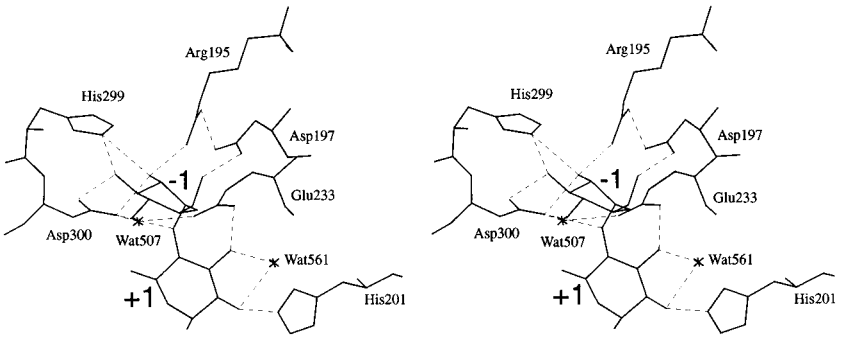

FIGURE 8: A stereo plot of the wild-type/acarbose complex structure in the direct vicinity of the three active site residues Asp197, Glu233, and Asp300. The side chains of these residues are believed to play a central role in the catalytic mechanism of human pancreatic α-amylase. Also drawn are the acarbose groups found in subsites −1 and +1, including the N-linked glycosidic bond that mimics the bond normally cleaved by HPA. From its observed conformation it is clear that Asp197 is ideally poised to act as the nucleophile in the cleavage reaction (Figure 2), while both Glu233 and Asp300 are positioned such that they could act in the role of the acid/base catalyst. Of particular interest is Wat507, which is located approximately midway between Glu233 and Asp300, and forms good hydrogen bonds with the side chains of both of these residues. This water molecule is a likely candidate to act as the nucleophile in the breakdown of the covalent bond formed to Asp197 during catalysis (Figure 2). Alternatively, it is possible that Wat507 could act directly as the acid/base catalyst in the reaction, with Glu233 and Asp300 simply acting to positionally assist this water molecule during the course of the reaction sequence.

complex involving the modified acarbose, the distance between this C1 carbon atom and the OD1 of Asp197 is 3.10 Å. The possibility that the side chain of Asp197 acts as the nucleophile in catalysis is also strongly implied from the kinetic results tabulated in Table 4, which show that a $\sim 10^6$-fold drop in catalytic activity is observed upon substitution of this residue with an asparagine.

Notably, the 2-hydroxyl of the valienamine moiety in subsite −1 is fully coordinated, interacting with three separate residues, His299, Asp300, and Arg195 (Figure 8). The

equivalent interactions are seen in the Michaelis and intermediate complexes of CGTase (*44*), while very similar interactions were seen in the acarbose complex of the TAKA amylase (*43*). This suggests that interactions at this 2-position are particularly important to catalysis, as has indeed been shown for other glycosidases (*45*, *46*). This is also consistent with the very slow turnover observed for the 2-deoxy-2-fluoro substrate (Table 4) since any important hydrogen-bonding interactions at the 2-position will have been severely compromised by the fluorine substitution.

Interestingly, the two residues Arg195 and Asn298, which both act as ligands in the nearby Cl^- ion binding site, are also located in the direct vicinity of the active site and form interactions to the active site residues Asp197 and Asp300, respectively. Bound Cl^- ion acts as an allosteric effector of HPA catalytic activity (*3*) and as the current results show may carry out this role by ensuring the proper conformation and/or ionization states of catalytic residues in the active site through joint interactions with ligand groups. Also directly in the active site region is the side chain of His201 which binds to atoms of the modified acarbose in subsite +1 (Figure 8). The carbonyl oxygen atom of this residue forms a ligand bond in the Ca^{2+} ion binding site of HPA (*2*). This calcium binding pocket is essential to the stability of the polypeptide chain fold of HPA. Our results indicate that neither of the bound Cl^- and Ca^{2+} ions, or the residues that form ligand bonds to these ions, shift significantly upon acarbose binding. Thus, these bound ions would appear to collectively prepare the proper geometric conformation of the active site for optimal activity rather than being direct participants in catalysis.

There are two segments of polypeptide chain that shift significantly upon binding of acarbose, and interestingly each of these segments is preceded by a key catalytic residue (Figure 6). One segment involves residues 233−240 and forms one side of the active site binding cleft, with particularly close interactions to the bound inhibitor in subsites −1 and −2 (see Figures 6 and 7). Apparently the presence of glycines 238 and 239 provides the necessary flexibility to this portion of the polypeptide chain to allow for the optimization of inhibitor interactions. Inhibitor binding in this region is accompanied by a modest drop in thermal factors for the main chain atoms of the residues involved.

A second segment of polypeptide chain that shifts upon acarbose binding comprises residues 303−311. In the free wild-type enzyme, these residues form a highly mobile surface loop that is substantially disordered in electron density maps (*2*, *29*). The primary structural anchor holding this mobile loop close to the enzyme surface is the active site residue Asp300. When acarbose is bound in the active site region, the residues of this loop shift to optimize their interactions with this inhibitor, and particularly extensive interactions are made in binding subsites −2 to +1 (Figures 6 and 7). The amino acid most affected by these shifts is His305, which forms a new hydrogen bond with the 2-hydroxyl of the sugar ring in binding subsite −2, and whose main chain amide group is also hydrogen bonded to the carbonyl group of Asp300. The requisite main chain flexibility in this region appears to be provided by a pair of glycine residues (Gly304 and Gly306). The inhibitor interactions formed by His305 and neighboring residues would appear to be responsible for the dramatic decrease in average main chain thermal factors for residues 298−309.

A surprising result from these studies concerns the effect that inhibitor binding has on the bulk of main chain thermal factors in the Ca^{2+} ion binding domain (domain B, Figure 5). Although from a positional perspective little change is observed, upon binding acarbose a substantial drop in main chain thermal factors is observed for most residues in this domain (residues 130−172). Although some of these residues (Leu165 and Thr168) form interactions with the modified acarbose bound in the active site cleft (Figure 6), these contacts are not extensive, and it is unclear what role domain B thermal factor changes play in either the substrate binding or catalytic functions of HPA.

(e) Structural Analyses of the D300N Variant of HPA. Substitution of an asparagine for the active site residue Asp300 causes little perturbation in the main chain conformation of HPA (Figure 6). The largest structural perturbation occurs at residue 300 where main chain atoms are shifted on average ∼1 Å. These shifts appear to be designed to accommodate the rotation of the side chain of Asn300 away from the active site cleft, to take up a more solvent-exposed position than that assumed by the normally resident aspartate. The observed changes in χ_1 and χ_2 side chain angles for residue 300 are 58° and 62°, respectively. The alternative positioning of the side chain of Asn300 also requires the readjustment of the nearby polypeptide chain. Most affected are residues 301−309, which are part of a mobile surface loop that forms extensive interactions to acarbose when it binds to the wild-type enzyme. A smaller positional shift is also seen for residues 235−239, likely as a result of modified interactions with the polypeptide chain in the region about residue 300.

Despite the relatively small perturbations apparent in the D300N variant structure of HPA, there are substantial differences in the interactions of residue 300 with other active site constituents. Thus, the greatly reduced activity ($\sim 10^3$-fold) of the D300N mutant therefore likely arises not only from its very limited capacity to act as an acid/base catalyst but also from the structural rearrangements engendered in the active site by this substitution. It is also of interest that in their more solvent-exposed position, the main and side chain atoms of Asn300 have substantially higher thermal parameters than do their Asp300 counterparts in wild-type HPA. Much higher thermal parameters are also observed for other neighboring residues positionally shifted in the D300N variant enzyme, including residues 238 and 301−310. Unexpectedly, a decrease in overall thermal parameters is observed for residues 130−170 which constitute the distant domain B (Figure 5) and form the bulk of the Ca^{2+} ion binding site. This change in thermal parameters is reminiscent of that observed upon binding of acarbose at the active site of the wild-type enzyme. It therefore suggests that the negative charge on Asp300 serves to destabilize the Ca^{2+} binding domain since removal of this charge, either by mutation (D300N) or by binding of a cationic ligand (protonated acarbose), reverses this effect.

(f) Structural Studies of the D300N HPA Variant/Acarbose Complex. As for the wild-type HPA/acarbose complex, refinement procedures for the D300N HPA variant/acarbose complex were initially focused solely on the protein portion of the complex. Following this, identification and interpreta-

tion of the nature of the bound inhibitor were undertaken using a difference electron density map. This map, and subsequent omit difference electron density maps, clearly showed the structure and placement of the bound inhibitor (Figure 4). The results obtained are unexpected and very different from those observed for the modified acarbose bound in the active site of wild-type HPA. As illustrated in Figures 4 and 6, in the D300N variant/acarbose complex only two sugar rings of a maltose unit can be discerned, and these bind in subsites −2 and −3 (Figure 1). This maltose unit can be uniquely identified in electron density maps on the basis of the placement of observed side chain groups. Electron density maps also show that subsites −1 through +2 remain unoccupied, and only water molecules are observed at these locations. This is in contrast to the conformation of the modified acarbose which forms a complex with wild-type HPA where the inhibitor spans subsites −3 to +2. It is clear from this work that substitution of an asparagine for Asp300 in HPA leads to significant differences in the manner in which acarbose interacts with the active site cleft of this enzyme and that residue 300 is a critical parameter in this process.

The manner in which the maltose group observed in the D300N variant/acarbose complex is bound in subsites −2 and −3 is nearly identical to that of the maltose component of modified acarbose bound to the wild-type enzyme (Figure 4). Note that in wild-type HPA, Asp300 makes a number of interactions with the acarbose sugar ring bound in subsite −1 (Figures 7 and 8), while in the D300N variant complex the only hydrogen bond formed is to the 2-hydroxyl group in subsite −2 (Figure 9).

Positionally, the impact of bound inhibitor on the main chain folding of D300N variant HPA is limited. The largest differences occur in the vicinity of residue 300 and likely reflect the formation of new interactions by Asn300 and His305 to the bound maltose group. Adjustments in the conformation of His305, which is part of a highly mobile surface loop near the active site, are substantial and very similar in both the wild-type and D300N variant HPA/acarbose complexes. Also inhibitor binding has little impact on the orientation of Asn300 (Figure 6) as reflected in the small overall average side chain displacement observed (0.70 Å) and the correspondingly small χ_1 and χ_2 side chain angle differences observed of 5° and 18°, respectively.

Three possible conclusions can be drawn with respect to the observed end product of acarbose binding to D300N HPA. One possibility is that acarbose has not been modified by the enzyme and is bound only via its (reducing end) maltose moiety with the pseudo-sugar acarviosine "disaccharide" disordered and therefore unseen. A second possibility is that acarbose has been cleaved to yield maltose and the acarviosine disaccharide, and that only the maltose moiety remains bound. A third possibility is that some form of transglycosylation has occurred and the disordered product is anchored in the active site by a maltose group. Transglycosylation or hydrolysis reactions seem unlikely, given the low catalytic activity of the D300N variant of HPA. However, with the very high effective concentration of enzyme in the crystal and the relatively long soak and data collection times, even a very low enzyme activity might yield enough product for stoichiometric (with protein) binding. On the other hand the poor electron density observed for the

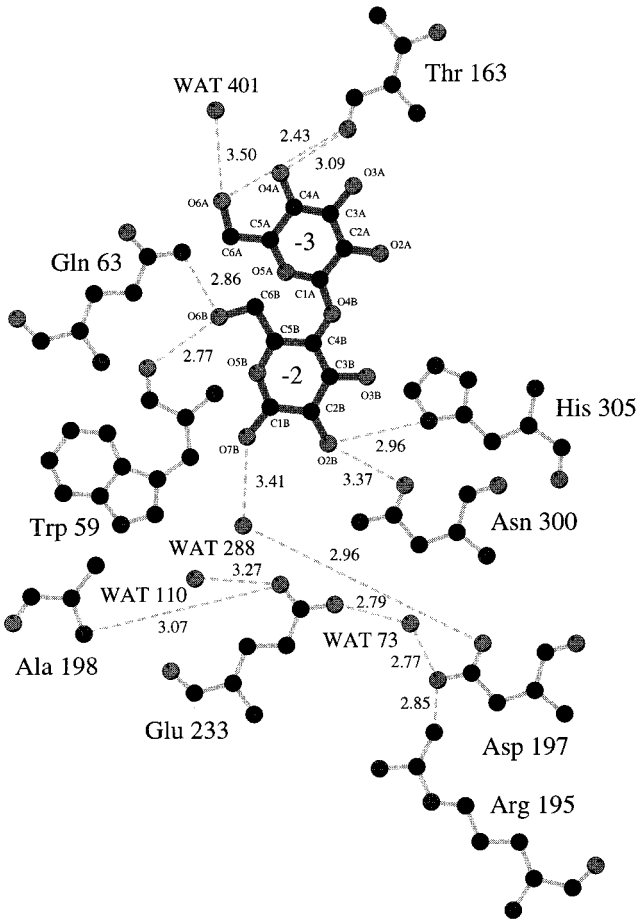

FIGURE 9: A diagrammatic illustration of the interactions formed by that portion of acarbose that can be visualized when bound in the active site of the D300N variant of HPA. As indicated, inhibitor atoms are found in binding subsites −2 and −3. Additional interactions formed by the active site residues Asp197, Glu233, and Asp300 are also illustrated. For clarity, individual non-hydrogen atoms of the bound inhibitor are labeled. Hydrogen bond interactions are indicated with dashed lines, and the lengths of these are given in angstroms. This figure was generated with the assistance of the programs HBPLUS (*48*) and Ligplot (*49*).

4-ring carbon and associated oxygen, along with the nearby 6-hydroxyl of the observed maltose unit, suggests that these atoms are partially positionally disordered. This is in contrast to the excellent definition of the equivalent atoms in the modified acarbose bound to wild-type HPA (Figure 4). Since these particular atoms would in turn form a part of the glycosidic link to the remainder of an uncleaved acarbose unit, which would also be disordered, these data are consistent with the possibility that an intact acarbose molecule is bound to the surface of the D300N variant form of HPA. Modeling studies do indicate that an intact acarbose molecule, anchored by its maltose end in subsites −2 and −3, would have sufficient room to take on a number of conformations in the active site cleft if it were projected outward from the enzyme surface. In the absence of any other form of product identification, which has thus far proved impossible in these systems (*43*), it is difficult to decide between the various options available.

All three potential interpretations of the observed structural data require that there be no significant binding of the acarviosine moiety across the −1 and +1 binding subsites. This must mean that interactions between Asp300 and the

inhibitor, presumably primarily those involving the imino nitrogen atom, are extraordinarily important, and that removal of this interaction abrogates binding in these subsites. This is in agreement with the weak K_i value of 0.4 mM found for acarbose inhibition of the D300N HPA variant enzyme compared to a value of 60 nM for the wild-type enzyme. Irrespective of which of the possible acarbose binding schemes is ultimately shown to explain the observed results, from the structural and kinetic data obtained for the D300N variant/acarbose complex it is clear that residue 300 plays a key role in ensuring the proper binding of substrates and inhibitors, and therefore the maintenance of optimal catalytic activity.

ACKNOWLEDGMENT

We thank Dr. R. Warren for a generous gift of endoglycosidase F-cellulose binding domain fusion protein and Mr. S. He for obtaining the mass spectra.

REFERENCES

1. Bernstein, F. C., Koetzle, T. F., Williams, G. J., Meyer, E. E., Jr., Brice, M. D., Rodgers, J. R., Kennard, O., Shimanouchi, T., and Tasumi, M. (1977) *J. Mol. Biol. 112*, 535−42.
2. Brayer, G. D., Luo, Y., and Withers, S. G. (1995) *Protein Sci. 4*, 1730−42.
3. Feller, G., le Bussy, O., Houssier, C., and Gerday, C. (1996) *J. Biol. Chem. 271*, 23836−23841.
4. Levitzki, A., and Steer, M. L. (1974) *Eur. J. Biochem. 41*, 171−180.
5. Gumucio, D. L., Wiebauer, K., Caldwell, R. M., Samuelson, L. C., and Meisler, M. H. (1988) *Mol. Cell. Biol. 8*, 1197−1205.
6. Meisler, M. H., and Ting, C. N. (1993) *Crit. Rev. Oral Biol. Med. 4*, 503−509.
7. Nishide, T., Emi, M., Nakamura, Y., and Matsubara, K. (1986) *Gene 50*, 371−372.
8. Ramasubbu, N., Paloth, V., Luo, Y. G., Brayer, G. D., and Levine, M. J. (1996) *Acta Crystallogr., Sect. D D52*, 435−446.
9. Truscheit, E., Frommer, W., Junge, B., Muller, L., Schmidt, D. D., and Wingender, W. (1981) *Angew. Chem., Int. Ed. Engl. 20*, 744−761.
10. Jenkins, D. J., Taylor, R. H., Goff, D. V., Fielden, H., Misiewicz, J. J., Sarson, D. L., Bloom, S. R., and Alberti, K. G. (1981) *Diabetes 30*, 951−4.
11. Taylor, R. H., Jenkins, D. J., Barker, H. M., Fielden, H., Goff, D. V., Misiewicz, J. J., Lee, D. A., Allen, H. B., MacDonald, G., and Wallrabe, H. (1982) *Diabetes Care 5*, 92−6.
12. Scheppach, W., Fabian, C., Ahrens, F., Spengler, M., and Kasper, H. (1988) *Gastroenterology 95*, 1549−55.
13. Uttenthal, L. O., Ukponmwan, O. O., Ghiglione, M., and Bloom, S. R. (1987) *Dig. Dis. Sci. 32*, 139−44.
14. Ruppin, H., Hagel, J., Feuerbach, W., Schutt, H., Pichl, J., Hillebrand, I., Bloom, S., and Domschke, W. (1988) *Gastroenterology 95*, 93−9.
15. Walter-Sack, I. E., Ittner-Holland, A., Wolfram, G., and Zoellner, N. (1986) *Eur. J. Clin. Pharmacol. 30*, 607−14.
16. Brogard, J. M., Willemin, B., Blickle, J. F., Lamalle, A. M., and Stahl, A. (1989) *Rev. Med. Intern. 10*, 365−74.
17. Henrissat, B. (1991) *Biochem. J. 280*, 309−316.
18. Henrissat, B., Callebaut, I., Fabrega, S., Lehn, P., Mornon, J. P., and Davies, G. (1995) *Proc. Natl. Acad. Sci. U.S.A. 92*, 7090−7094.
19. Henrissat, B., and Davies, G. (1997) *Curr. Opin. Struct. Biol. 7*, 637−644.
20. Qian, M., Haser, R., Buisson, G., Duee, E., and Payan, F. (1994) *Biochemistry 33*, 6284−6294.
21. Larson, S. B., Greenwood, A., Cascio, D., Day, J., and McPherson, A. (1994) *J. Mol. Biol. 235*, 1560−1584.
22. Gilles, C., Astier, J. P., Marchis-Mouren, G., Cambillau, C., and Payan, F. (1996) *Eur. J. Biochem. 238*, 561−9.
23. Hayashi, M., Hashimoto, S., and Noyori, R. (1984) *Chem. Lett.* 1747−1750.
24. Lindhorst, T. K., Braun, C., and Withers, S. G. (1995) *Carbohydr. Res. 268*, 93−106.
25. Junneman, J., Theim, J., and Pedersen, C. (1993) *Carbohydr. Res. 249*, 91−94.
26. Clark-Still, W., Kahn, M., and Mitra, M. (1977) *J. Org. Chem. 43*, 2923−2926.
27. Hayashi, M., Hashimoto, S., and Noyori, R. (1984) *Chem. Lett.* 1747−1750.
28. Burk, D., Wang, Y., Dombroski, D., Berghuis, A. M., Evans, S. V., Luo, Y., Withers, S. G., and Brayer, G. D. (1993) *J. Mol. Biol. 230*, 1084−1085.
29. Rydberg, E. H., Sidhu, G., Vo, H. C., Hewitt, J., Côté, H. C. F., Wang, Y., Numao, S., MacGillivray, R. T. A., Overall, C. M., Brayer, G. D., and Withers, S. G. (1999) *Protein Sci. 8*, 635−643.
30. Kunkel, T. A., Roberts, J. D., and Zakou, R. A. (1987) *Methods Enzymol. 154*, 367−382.
31. Sanger, F., Nicklen, S., Coulson, A. R. (1977) *Proc. Natl. Acad. Sci. U.S.A. 74*, 5463−5467.
32. Leatherbarrow, R. J. (1990) Erithacus Software Ltd., Staines, U.K.
33. McCarter, J. D., Adam, M. J., Braun, C., Namchuk, M., Tull, D., and Withers, S. G. (1993) *Carbohydr. Res. 249*, 77−90.
34. Otwinowski, Z., and Minor, W. (1997) *Methods Enzymol. 276*, 307−326.
35. Navaza, J. (1994) *Acta Crystallogr. A50*, 157−163.
36. Brünger, A. T. (1992) *X-PLOR Version 3.1: A system for X-ray crystallography and NMR*, Yale University Press, New Haven, CT.
37. Jones, T. A., Zhou, J.-Y., Cowan, S. W., and Kjeldgaard, M. (1991) *Acta Crystallogr. A47*, 110−119.
38. Luzzati, P. V. (1952) *Acta Crystallogr. A50*, 803−810.
39. Seigner, C., Prodanov, E., and Marchis-Mouren, G. (1987) *Biochim. Biophys. Acta 913*, 200−209.
40. Okada, G., Genghof, D. S., and Hehre, E. J. (1979) *Carbohydr. Res. 71*, 287−98.
41. Withers, S. G., and Aebersold, R. (1995) *Protein Sci. 4*, 361−372.
42. McCarter, J. D., Yeung, W., Chow, J., and Dolphin, D. (1997) *J. Am. Chem. Soc. 119*, 5792−5797.
43. Brzozowski, A. M., and Davies, G. J. (1997) *Biochemistry 36*, 10837−45.
44. Uitdehaag, J. C. M., Mosi, R., Kalk, K. H., van der Veen, B. A., Dijkhuisen, L., Withers, S. G., and Dijkstra, B. W. (1999) *Nat. Struct. Biol. 6*, 432−6.
45. Namchuk, M. N., and Withers, S. G. (1995) *Biochemistry 34*, 16194−16202.
46. Notenboom, V., Birsan, C., Nitz, M., Rose, D. R., Warren, R. A. J., and Withers, S. G. (1998) *Nat. Struct. Biol. 5*, 812−818.
47. Robyt, J. F., and French, D. (1970) *J. Biol. Chem. 245*, 3917−27.
48. McDonald, I. K., and Thorton, J. M. (1994) *J. Mol. Biol. 238*, 777−793.
49. Wallace, A. C., Laskowski, R. A., and Thornton, J. M. (1995) *Protein Eng. 8*, 127−134.

BI9921182